

Plausible failure mechanisms of wildlife-damaged earth levees: insights from centrifuge modeling and numerical analysis

Gholamreza Saghaee, Ahmad A. Mousa, and Mohamed A. Meguid

Abstract: Earth levees are subject to a wide range of wildlife intrusion patterns that cause mass removal and subsequent serious deformations. Such invasive activities leave the body of an earth embankment with burrow systems too complex to map and model using conventional techniques. This study investigates the impact of different idealized configurations of animal burrows on the geotechnical performance of levees. For this purpose, centrifuge testing was conducted on homogenous scaled-down 1 horizontal : 1 vertical (1H:1V) levee models built from silty sand material. Modeling involved introducing horizontal cylinder-shaped waterside and landside burrows at different elevations within the levee section. The reference (intact) and deteriorated levee models were subject to a centrifugal acceleration of 35g, which was kept constant as the water level behind the levee model was gradually increased. The deformation profile of the model was tracked, and the crest displacements were concurrently measured. Miniature pore pressure transducers (PPTs) embedded within the levee body provided pore pressure measurements. A three-dimensional finite element model was developed to investigate the hydraulic performance and verify the failure patterns of the deteriorated levees. Compared with an intact levee, the presence of animal intrusions was found to increase the exit hydraulic gradient for both waterside and landside intrusions. Lower animal burrows appeared to cause larger exit gradients than higher ones. Similarly, waterside burrows exhibited a notably higher pore pressure and larger hydraulic gradient. Waterside damage resulted in a quicker and more violent failure than landside burrows. The failure mechanisms for both the waterside and landside burrows are dissimilar despite their similarly abrupt nature.

Key words: stability of earth structures, geotechnical performance of levees, wildlife intrusion patterns, centrifuge modeling, seepage analysis.

Résumé : Les levées de terre sont soumises à un large éventail de modes d'intrusion de la faune qui provoquent des déformations graves et des pertes de masse. Ces activités envahissantes quittent le corps de remblais de terre avec des systèmes de complexité terrier au-delà de la modélisation et de la cartographie traditionnelle. Cette étude examine l'impact de différentes configurations idéalisées des terriers d'animaux sur la performance de géotechnique de digues. À cette fin, on a effectué des tests de centrifugeuse à échelle réduite homogène sur modèles de digues à l'échelle 1 horizontale : 1 verticale (1H : 1V) construites à partir de matériaux de sable limoneux. La modélisation consiste de l'introduction d'un cylindre horizontal et côté ville au bord de l'eau en forme de terriers à différentes hauteurs dans la section de digue. La référence (intacts) et détérioré de modèles de levée ont été soumis à une accélération centrifuge de 35g, qui a été maintenu constant comme le niveau d'eau derrière le modèle de digue a progressivement augmenté. Le profil de déformation du modèle a été suivi et les déplacements piques ont été mesurés simultanément. Des capteurs de pression interstitielle miniatures (PPTs) intégrés dans le corps de digue ont fourni des mesures de pression interstitielle respective. Un modèle par éléments finis en trois dimensions a été développé pour étudier le rendement hydraulique et vérifier les modes de défaillance des digues détériorés. Par rapport à la digue intacte, la présence d'intrusions d'animaux a été trouvée augmenter le gradient hydraulique de sortie pour les intrusions de côté ville et au bord de l'eau. Les terriers inférieurs d'animaux apparaissent à causer les plus grandes sorties que les gradients supérieurs. De même, les terriers près de l'eau présentaient une pression interstitielle notamment plus élevée et un gradient hydraulique plus grand. Les dommages au bord de l'eau ont donné une procédure plus rapide et plus violente que celle associée au cas du côté de sol. Les mécanismes de rupture pour les terriers et côté ville au bord de l'eau sont très différents en dépit de leur nature semblable brutale. [Traduit par la Rédaction]

Mots-clés : stabilité des structures en terre, performance géotechnique de digues, modes d'intrusion par la faune, analyse d'infiltration, modélisation par centrifugation.

Introduction

Damage to earthen structures caused by invasive wildlife activities is observed worldwide. Such natural occurrences are often associated with economic losses to infrastructure and property. Animal burrows have been known to negatively influence the hydraulic performance of earth dams and in severe cases could lead to a loss of structural integrity. Failures and losses related to

animal activities in earth structures are discussed in further detail by Bayoumi and Meguid (2011). Damage caused by nuisance activities could remain concealed for a long time, until the safety of an earth structure is jeopardized (Blach et al. 2010).

Breaches of earth dams are driven by a variety of actions, including excessive forces from retained water (floods), low-strength materials, and seismic activities. The consequences of wildlife activities

Received 7 September 2016. Accepted 8 May 2017.

G. Saghaee and M.A. Meguid. Department of Civil Engineering and Applied Mechanics, McGill University, Montréal, QC H3A 0C3, Canada.

A.A. Mousa. School of Engineering, Monash University, Selangor, Malaysia.

Corresponding authors: Mohamed A. Meguid (email: mohamed.meguid@mcgill.ca); Ahmad A. Mousa (email: ahmad.mousa@monash.edu).

Copyright remains with the author(s) or their institution(s). Permission for reuse (free in most cases) can be obtained from RightsLink.

in levees can be categorized as structural damage, surface erosion, or hydraulic alterations (FEMA 2005). These adverse outcomes are often related. Changes to hydraulic performance is one of the most common causes of failure in earthen structures and typically lead to internal erosion and piping (Fell et al. 2003). Although internal erosion naturally occurs in solid earth structures, its consequences are exacerbated by cracks or cavities within the soil mass.

Controlling seepage through earth dams and levees is an important design requirement to prevent excessive uplift pressures, piping, and erosion of material through losses into cracks, joints, and cavities (Sherard et al. 1963; Arulanandan and Perry 1983; FEMA 2011; Sherard and Dunnigan 1985). Extensive research has been done on intact earth structures to study the mechanisms of piping (van Beek et al. 2010, 2011; Sellmeijer et al. 2011; Zhou et al. 2012), erosion (Bonelli and Brivois 2008; Boukhemacha et al. 2011; Xu et al. 2012), and overtopping (Schmocker and Hager 2012; Sharp and McAnally 2012). A significant amount of the literature in the area of wildlife investigates the ecological impact of animal activities and habitat (Bayoumi and Meguid 2011). However, studies investigating potential failure mechanisms of earth structures due to invasive wildlife activities are scarce. Visual inspection of wildlife damage in earth structures might leave an average observer with the false impression that they are erratic and random. The convoluted nature of these burrow systems in earth dikes and dams hides ingenious engineering that is not well understood, and their complexity may account for the limited studies of their impact. Wildlife dwelling in these structures typically have a strong preference of intruding from either the waterside or the landside but occasionally intrude from both sides (Bayoumi and Meguid 2011). Predation and other ecological wildlife activities have a significant impact on the location and geometry of burrow systems.

Scope

Understanding the failure mechanism of damaged earth structures — even at an abstract level — is pivotal for sound post-failure analysis and plausibly for adequate design of earth structures. This research investigates the impact of location and elevation of animal burrows on the behavior of earth levees. An array of equidistant horizontal cylindrical burrows is introduced at different elevations within a centrifuge levee model. This arbitrary damage configuration is supported by the dominance of near-horizontal animal burrows in earth structures (Chlaib et al. 2014). Both waterside and landside attacks are closely examined by monitoring the surface movement, global deformation, and changes in pore pressure distribution due to the introduction of these cylindrical burrows.

A description of the physical model, summary of the methodology used to introduce animal burrows within the model, and details of the centrifuge testing are presented in this paper. The test results of an instrumented intact levee model, including surface displacements and pore pressures, are summarized and compared with those measured for deteriorated levee cases. The effects of the configuration of animal burrows on the hydraulic performance and stability of levees are discussed. Three-dimensional (3D) finite element (FE) analyses are used to support the hypothesized reasons for the alterations to the phreatic surface and the failure mechanisms of the deteriorated levees.

Experimental program

Hori et al. (2007) successfully used the Kasama soil (silty sand) for centrifuge modeling of earth dams (Table 1). Its weak cohesion provides favorable conditions for invasive wildlife activities. The low to medium plasticity offers wildlife a reasonable balance between stability of cavities and relative ease in digging. A side slope of 1 horizontal : 1 vertical (1H:1V) seems to support initial stability

Table 1. Characteristics of Kasama soil.

Property	Values
Specific gravity, G_s	2.67
Moisture content (%)	30
Liquid limit, LL	14.1
Plastic limit, PL	10.9
Dry density, γ_d (max) (kN/m ³)	13.8
Optimum moisture content, OMC (%)	27.5
Saturated density, γ_{sat} (kN/m ³)	16.8
Unsaturated density, γ_{unsat} (kN/m ³)	14.1
Elastic modulus, E (MPa)	14
Poisson's ratio, ν	0.25
Friction angle, ϕ' (°)	32
Dilation angle, ψ (°)	0
Effective cohesion, c' (kPa)	5.9
Hydraulic conductivity, k (m/s)	3.8×10^{-5}

of the levee model and simultaneously — from an experimental feasibility standpoint — provides an ample chance of failure in the case of a deteriorated levee (Saghaee et al. 2016). Although a relatively steep slope is uncommon for engineered earth dams, this configuration allows for viably investigating both serviceability (prior to failure) and ultimate limit states. A line of horizontal equispaced cylindrical burrows was introduced at different elevations within the levee section. Each test case had one set of burrows at the same elevation on either the waterside (WB) or landside (LB) of the model (Fig. 1a). Centrifuge modeling enabled close examination of the animal burrows' effect on the stability and hydraulic performance of the levee section in a controlled environment. For benchmarking, an intact levee section was tested in a similar fashion. The details of the experimental program reported by Saghaee et al. (2016) are summarized below.

Setup and burrow configuration

A 1:35 scaled-down section was built to model a levee 5 m high with a 4 m crest width and 1H:1V side slopes. The Kasama soil was compacted in the centrifuge box to a moisture content of approximately 30% in nine 25 mm thick lifts to the desired height. To eliminate the risk of disturbance, the levee section was shaped carefully and incrementally by removing the soil (excavation) to attain the predefined levee model configuration (Fig. 1a). Thin-wired 100 psi (689.5 kPa) pore pressure transducers (PPTs — Model GE Druck PDCR 81-347) were placed during construction at pre-selected locations along the centerline of the model to monitor pore pressure changes during the test (Fig. 1a). The use of sufficiently long PPT wires minimized the impact of interference on the measured deformations. The wires were monitored for unusual tension or movement during the experiments.

Animal burrows were modeled as cylindrical cavities using six stainless steel rods of 8.5 mm diameter, spaced 50 mm apart (Fig. 1b). At a 35g acceleration level, a customized pullout system gradually extracted the pre-installed rods during the centrifuge flight. This method successfully introduced burrows at depths (D_B) of 0.5 and 0.75 of the levee height (H_L). The model embankment (143 mm height and 400 mm width) experienced gradual spinning up to the targeted centrifugal acceleration (35g). The centrifuge box containing the model was equipped with a transparent face to allow for visual monitoring of the deformations during testing (Fig. 2). The levee construction procedure and further modeling details are provided by Saghaee et al. (2012a, 2012b).

The configuration of the model arbitrarily mimics conditions in which clustered animals (of high population) exercise invasive activities. The burrow length and diameter are inspired by the typical activities of large digging carnivores. For example, the American badger is known to dig slightly elliptical openings averaging 20–30 cm in diameter and extending horizontally up to 9 m in the ground (Bayoumi and Meguid 2011). Accurate modeling of a real

Fig. 1. Model configurations: (a) geometry and location of PPTs (P1–P3) and (b) plan view of the model with waterside burrows (Saghaee et al. 2016). [Color online.]

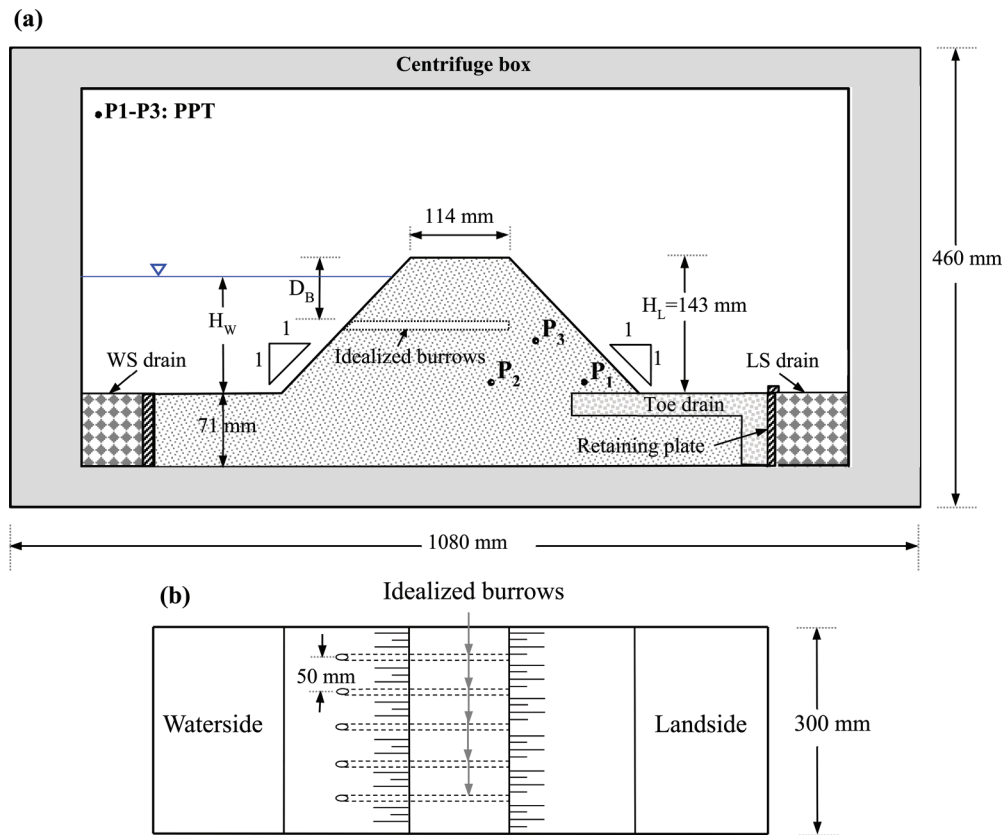
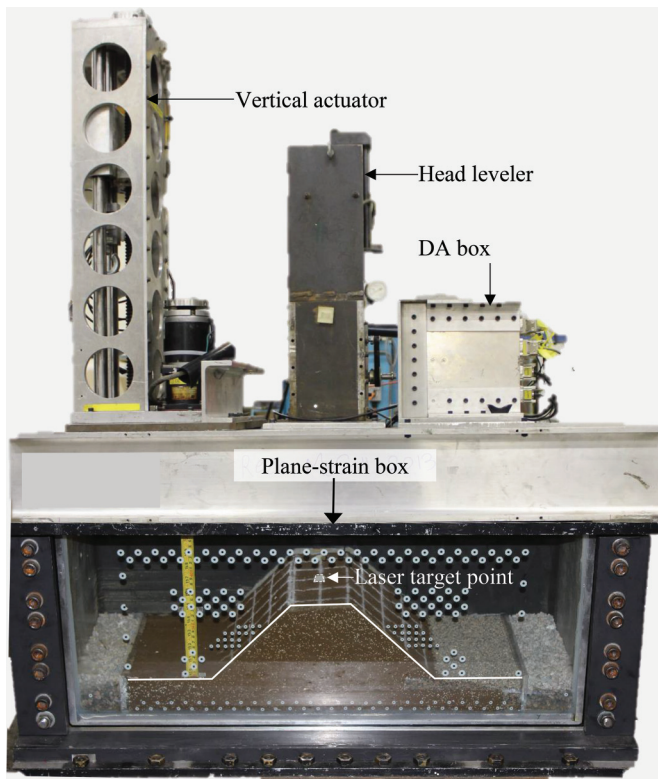


Fig. 2. Test setup installed on plane-strain centrifuge box. [Color online.]

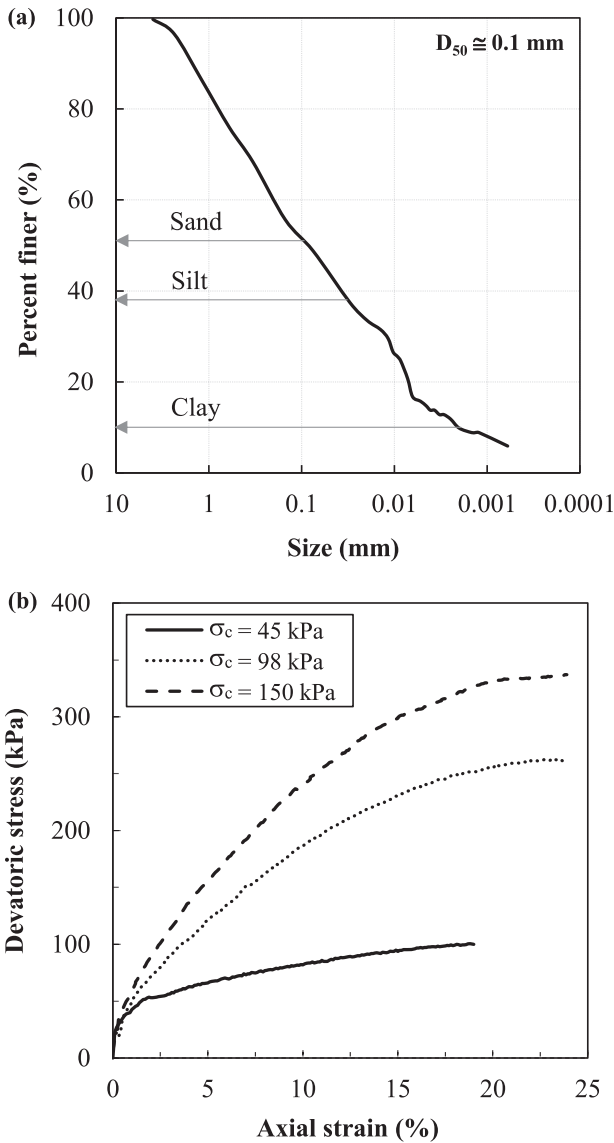


burrow network can be tedious and time-consuming; therefore, a row of cavities is deemed to be qualitatively representative of sufficient damage that would eventually lead to failure. This study seeks understanding of seepage patterns and failure mechanisms of deteriorated earth structures at the conceptual level.

Material characterization

The Kasama soil was fully characterized — via index, particle size distribution, standard proctor, shear strength, and hydraulic conductivity tests — for model construction and numerical simulation. Figure 3a depicts the gradation curve for Kasama soil. The material is classified as silty sand (SM) using the Unified Soil Classification System (ASTM 2011). Constant head permeability tests suggested a coefficient of hydraulic conductivity of approximately 3.8×10^{-5} m/s. The levee model was constructed inside the centrifuge box using the compaction and excavation technique. This method involves two steps: (i) placement and compaction of the soil in equal thickness lifts (layers) up to the desired height and (ii) removal of the soil (excavation) to shape the levee cross section. This levee construction procedure was strictly followed for both the intact and the deteriorated levee models. Sagheea et al. (2016) discussed in further detail the compaction test in relation to the construction of the model. Drained strength and stiffness of the soil used to build the levee model were evaluated for consolidated, drained triaxial tests at three confining pressures: 50, 150, and 200 kPa (Fig. 3b). Soil specimens were prepared in a mold and tamped in four layers, following a procedure similar to that used to build the levee. Hydraulic conductivity was also measured and was found to be about 3.8×10^{-5} m/s. The average moisture content of the prepared specimens was found to be approximately 30%, which is comparable to that of the levee model before the water level was raised. The soil properties and parameters are summarized in Table 1.

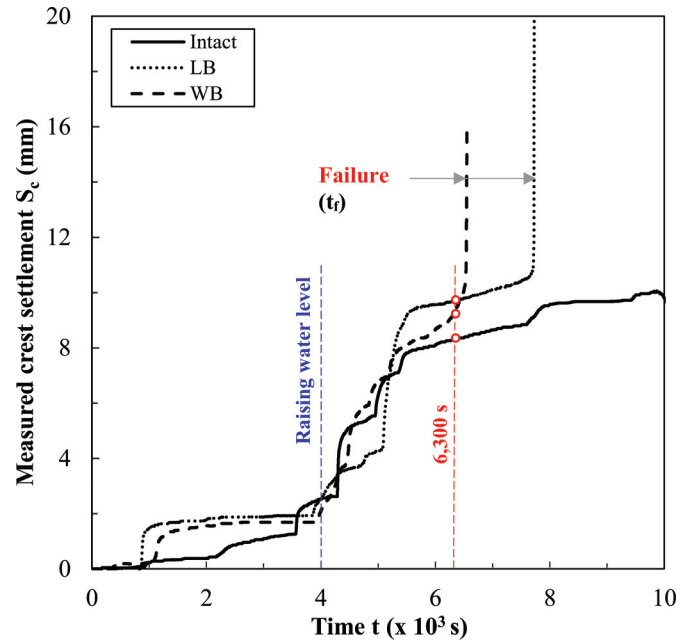
Fig. 3. Kasama soil characterization: (a) particle-size distribution and (b) triaxial consolidated, drained stress–strain curves for confining pressure of 45, 98, and 150 kPa.



Testing procedure

The centrifuge testing started by spinning up the model to an initial acceleration of 10g. A payload (including the setup and the model) of about 800 kg reached the targeted centrifuge acceleration (35g) at an angular speed of 78 rpm. The overall performance of the model appeared to be adequate, with the monitoring instruments functional at this acceleration level. The maximum error associated with stress nonlinearity (approximately 0.7%) fell within acceptable limits (Taylor 1995). Gradual pullout of rods commenced at a rate of 0.33 mm/s immediately upon reaching the maximum acceleration. The negligible settlement observed at the crest during the pullout indicated repeatability of cavity introduction and initial conditions. Following rod removal from the levee body, the water level on the waterside was gradually raised, beginning at elapsed time of 4000 s, using a water pump. The process of increasing the water level lasted for about 200 s, allowing for steady-state conditions (constant PPT readings) to be reached for each 20 mm increment. The water was then maintained at a target level (H_w) using an onboard head leveler and monitored using a PPT installed within the main drain.

Fig. 4. Measured changes in crest settlement with increase in water level for intact levee, levee with LB, and levee with WB. [Color online.]



Monitoring scheme

Digital photography captured numerous images of soil deformations. Three high-resolution digital cameras (10.0 megapixel, 6x optical zoom) were affixed outside the centrifuge box to monitor the planar soil deformation through the transparent wall. Two cameras closely monitored waterside and landside slopes, and the central camera covered the whole levee model, including the foundation. The progression of geometrical changes of the cross section was snapshotted at 5 s intervals. A high-definition camcorder continuously monitored the profile of the model. Additionally, two laser linear variable differential transformers (LVDTs) were used to measure the crest settlement along the centerline of the model. High-resolution still imaging during the centrifuge flights allowed for post-processing of deformations using particle image velocimetry (PIV) analysis (White et al. 2003). A thin soil layer near the transparent wall was mixed with 5% polystyrene beads 1 mm in diameter to texturize the soil and allow for the deformation to be accurately measured.

Observations

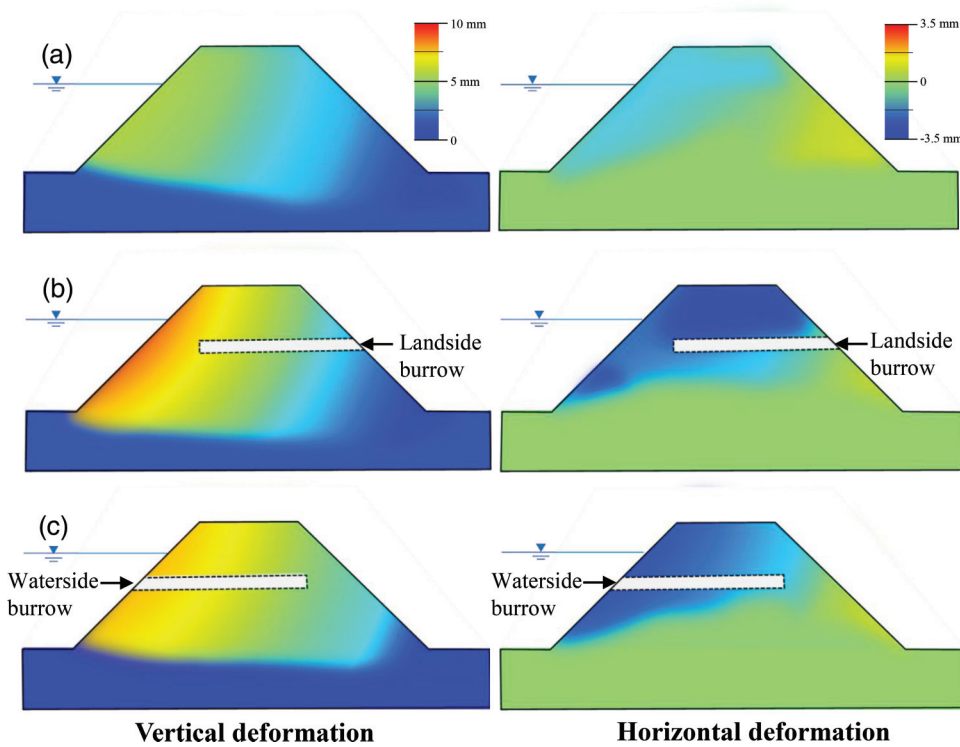
The study investigated the impact of the burrows' configuration (attack side and elevation) on the performance of the modeled levee. The following observations are used to identify the nature of failure in deteriorated levees. The deformation, hydraulic performance, and failure progress of the deteriorated models are separately discussed.

Deformation field

The measured crest settlement for both deteriorated models (WB and LB) are depicted alongside that of the intact model in Fig. 4. All cases experience a gradual increase in crest settlement up to approximately 2 mm prior to elevating the water level (at time $t = 4000$ s). An abrupt increase in the crest settlement occurs shortly after the water level is raised. The deteriorated models exhibit a distinctive failure response commencing at elapsed time of about 6000 s (Fig. 4). The WB and LB models experienced excessive and abrupt settlement followed by rapid failure at elapsed times of approximately 6500 and 7700 s, respectively. Comparatively, the crest settlement measured for the intact levee pla-

Can. Geotech. J. Downloaded from www.nrcresearchpress.com by MCGILL UNIVERSITY on 09/22/17 For personal use only.

Fig. 5. Contour plot of cumulative vertical and horizontal deformations due to rising water level from $t \cong 4000$ to 6300 s for (a) intact levee, (b) levee with LB, and (c) levee with WB. [Color online.]



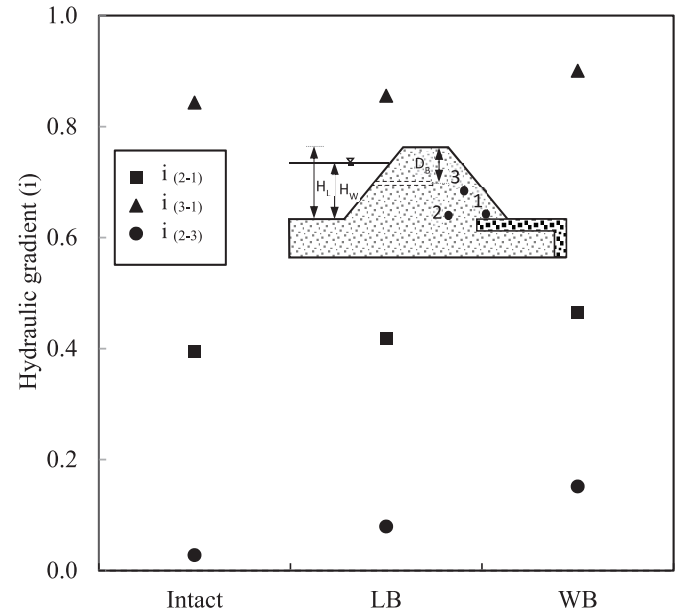
teated at about 9 mm and showed no signs of distress up to the end of the experiment.

Contours of the vertical and horizontal deformations for all cases are post-processed using PIV analysis during the period in which the water level was raised (from $t \cong 4000$ to 6300 s). The cumulative vertical and horizontal displacements from PIV analysis are illustrated in Fig. 5. Positive vertical and horizontal displacements indicate downward and lateral movements toward the landside, respectively. As expected, the maximum vertical and horizontal deformations of intact levee cross section are smaller than those of the deteriorated models (Figs. 5b and 5c). Although they appear similar, the contours of the vertical displacements (subsidence) for the WB model suggest higher settlement than the LB model. This is in line with the trends of crest settlement observed within the same time interval (Fig. 4). The LB model exhibited larger vertical deformations at the closed end of the burrows and around the waterside toe (Fig. 5b). Horizontal deformations of the intact model are insignificant, with an average hovering around zero displacement. The top of the foundation of the deteriorated models demonstrated moderate to high vertical settlements on the order of 4–8 mm, increasing toward the waterside toe. This deformation pattern stands behind the noted tilt of the model toward the waterside. The horizontal deformation contours for WB and LB models are similar, with larger horizontal deformations around the waterside slope. Based on the observed contours, the average horizontal displacements for the deteriorated models are around 40% of their vertical displacements. Considering the modeling scale at 35g, vertical and horizontal displacements of a full-size levee section would be approximately 25 and 10 cm, respectively.

Hydraulic response

Pore pressure readings obtained during the experiment allowed the hydraulic response of the model to be gauged. As depicted in Fig. 1a, the PPTs measured pore pressures at three locations within the landside toe: P1, P2, and P3. The previously described levee

Fig. 6. Hydraulic gradients near the exit for deteriorated models with burrows at mid-height versus intact model.



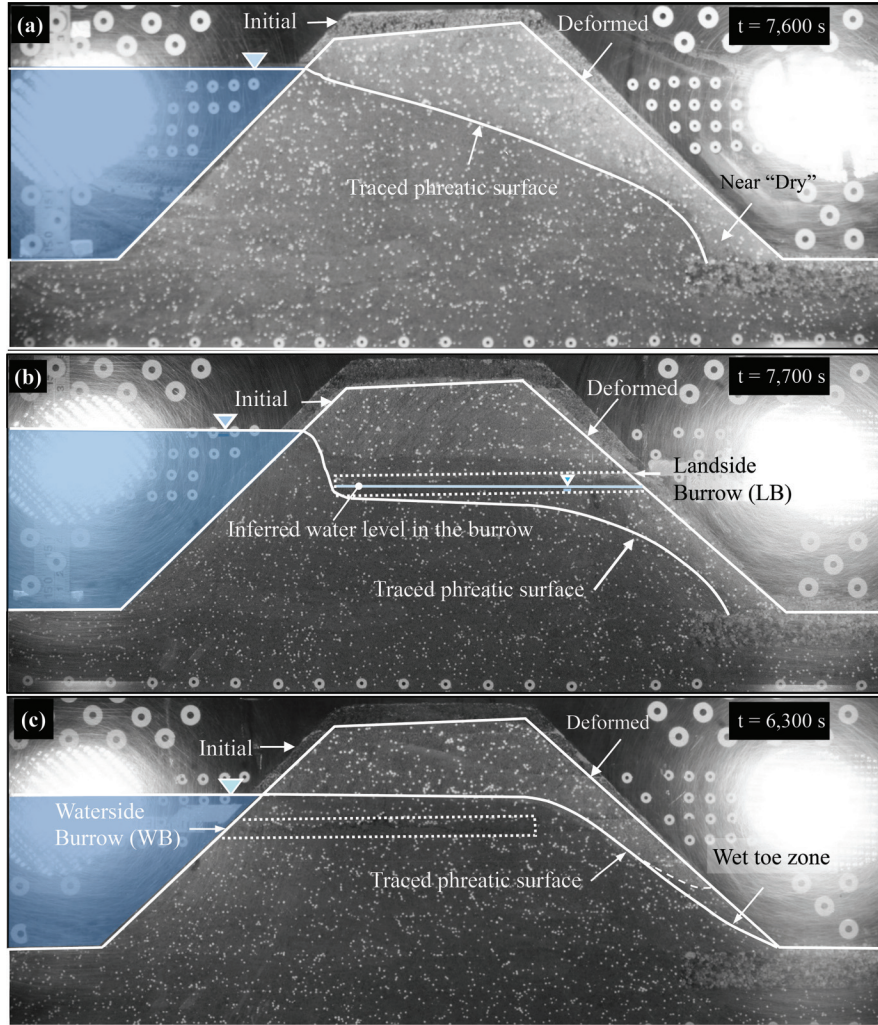
deformations might result in slight changes in the elevations of the installed PPTs. The total head (h_t) was calculated based on the corrected elevation of the PPT after settlement (z_{cor}) as follows:

$$(1) \quad z_{cor} = z_o - \Delta z$$

$$(2) \quad h_t = z_{cor} + h_p$$

Can. Geotech. J. Downloaded from www.nrcresearchpress.com by MCGILL UNIVERSITY on 09/22/17 For personal use only.

Fig. 7. Inferred phreatic surface for levee models: (a) intact, (b) LB (prior to failure), and (c) WB (prior to failure). [Color online.]



where z_0 is the initial height of the PPT above the datum (levee base), Δz is the corresponding settlement (linearly interpolated), and h_p is the pressure head.

Figure 6 illustrates the impact of attack side on the hydraulic gradient, i , for the intact, LB, and WB models. The figure shows the gradients for the deteriorated models with burrows at mid-height. The hydraulic gradient near the exit toe was calculated as the quotient of the total head difference and the distance between the respective PPTs. Compared with the intact case, the hydraulic gradient of the deteriorated models is higher, increasing toward the landside toe drain. The hydraulic gradient of the WB case was greater than that of the LB case. Although these gradients could be different from local gradients, they still indicate the effect of the burrow configuration on hydraulic response.

Figure 7 depicts the traced (approximate) phreatic surfaces for the three cases overlain on high-resolution still images. The slightly darker shades indicate the wet soil (below the phreatic surface), whereas the light shades represent the partially saturated and drier regions (above the phreatic surface). The intact model exhibits a classical steady-state flow of water, with the phreatic surface between the maximum retained water level (waterside) and the toe drain (Fig. 7a). In contrast, the presence of cavities in the deteriorated levees alters the classical seepage path (Figs. 7b and 7c). For the LB model, the water seeped through the waterside slope and preferentially collected in the burrows. The phreatic surface was parallel to the burrows within the levee prior

Fig. 8. Effect of burrow depth on hydraulic gradient near the exit for WB at $H_w = 94$ mm. [Color online.]

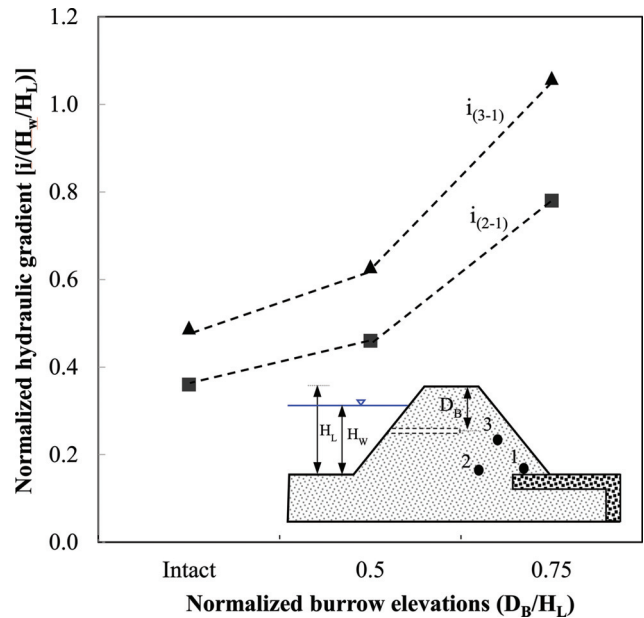


Fig. 9. Failure of levee with LB for $t/t_f =$ (a) 0.431, (b) 0.833, (c) 0.847, (d) 0.880, (e) 0.994, and (f) 1.00. [Color online.]

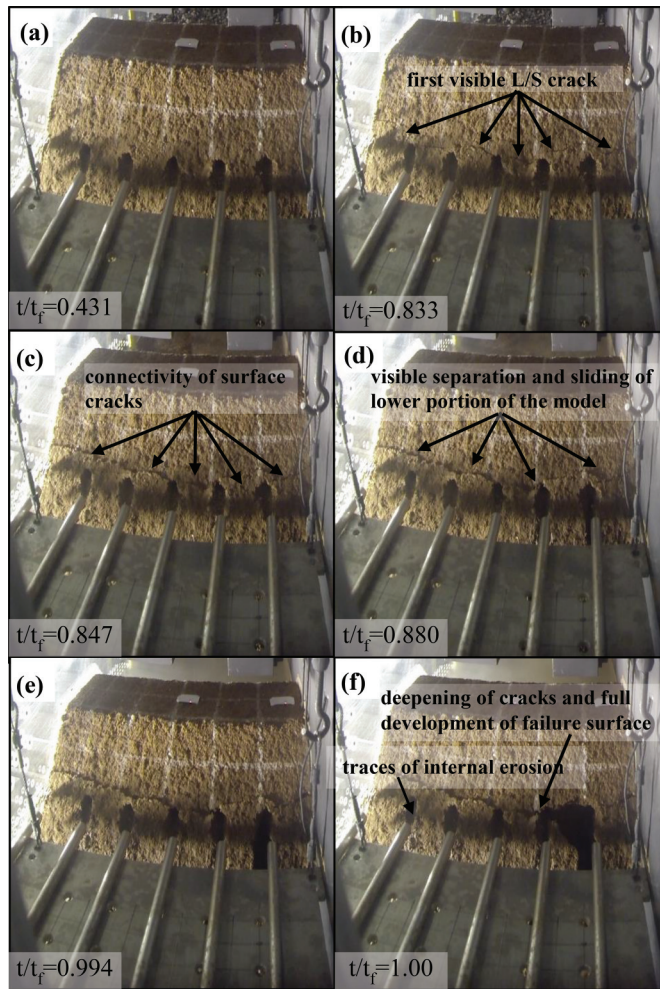
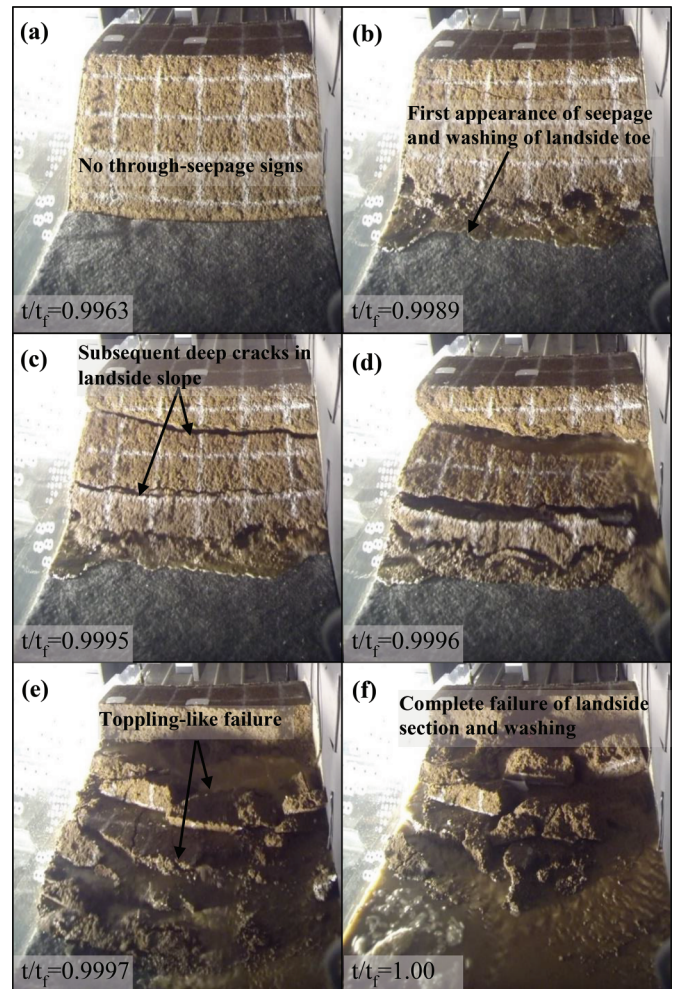


Fig. 10. Failure of levee with WB for $t/t_f =$ (a) 0.9963, (b) 0.9989, (c) 0.9995, (d) 0.9996, (e) 0.9997, and (f) 1.00. [Color online.]



to running parallel to the landside slope toward the landside toe (Fig. 7b). In the case of WB, the burrows allowed direct access to water with minimal head loss along their length. The preferential near-horizontal flow path created early in the seepage process resulted in a rise in the phreatic surface, which eventually exited near the toe of the model (Fig. 7c). Compared with the LB case, the higher profile of the phreatic surface for the WB model explains the higher measured exit gradients (Fig. 6).

Depending on the dominating wildlife species at the levee location, attacks from the waterside could target lower elevations. Thus, a line of burrows at the bottom quarter ($D_B/H_L = 0.75$) of the model's height was introduced. Figure 8 depicts the effect of the burrow elevation on the hydraulic performance of the deteriorated levee. The normalized hydraulic gradient was used for this purpose. The measured gradient, i , is divided by H_w/H_L to relate head loss to water levels on the waterside. The low-elevation burrows ($D_B/H_L = 0.75$) yielded a hydraulic gradient of about twice that of the mid-height burrows ($D_B/H_L = 0.5$) (Fig. 8). Like the raw hydraulic gradient, the normalized gradient provides a relative measure of the hydraulic performance for deteriorated levees.

Failure progress

Still imaging of the models taken during the centrifuge flights was used to conceptualize the progress of failure. The LB and WB cases show distinct failure mechanisms despite their similarly abrupt nature. The following summarizes the key observations for both models.

The key characteristics and signs of failure of the LB levee model were captured in selected images from a time stamp (TS = t/t_f , where t_f is the time to failure) of 0.431–1.0 (Fig. 9). The first visible landside crack appeared at a TS of 0.833 and laterally propagated as isolated distresses near the apex of burrows, as shown in Fig. 9b. Interconnectivity of cracks on the landside was spotted at a TS of 0.847 (Fig. 9c). Sliding and separation of the bottom half of the landside slope seemed to commence at a TS of 0.880 (Fig. 9d). Further deepening of the cracks eventually led to complete loss of structural integrity at a TS of 1.0 (Fig. 9f).

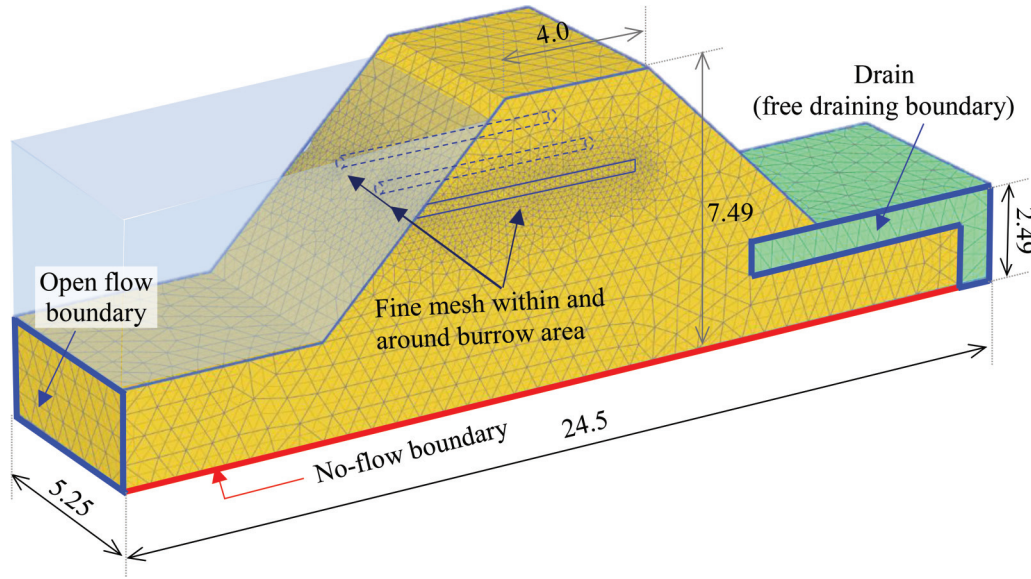
Until a TS of 0.9963 the WB model showed no signs of through-seepage (Fig. 10a). The rapid distress signs were captured in selected images from a TS of 0.9989 to 1.0 (Figs. 10b–10f). The first appearance of seepage and washing of the landside toe commenced at a TS of 0.9989 (Fig. 10b). Subsequent deep horizontal cracks in the landside slope (Figs. 10c and 10d) propagated swiftly in a toppling mode (Fig. 10e) until complete failure. At this stage, half of the landside section was washed almost instantly, as illustrated in Fig. 10f.

Numerical analyses

Model description

Three-dimensional FE analysis was performed using Plaxis 3D software (Plaxis 2015) to further support the visual observations of the physical model. This approach (numerical simulation) was particularly important given the distribution and shape of the

Fig. 11. Vertical cross section through middle burrow of finite element model: geometry (in m) and boundary conditions. [Color online.]



burrows within the body of the model as well as the possible scale effects in the centrifuge model. A full-scale numerical model that captured the geometric features of the levee and the burrows was developed. The seepage analysis assumed a homogenous isotropic material under steady-state conditions. The stress and stability analyses were performed using the Mohr–Coulomb failure criterion. Using geometrical symmetry, only half of the embankment was modeled, to reduce the mesh size and the computation time needed for the analysis. The FE model dimensions, mesh, and hydraulic boundary conditions are shown in Fig. 11. To reduce the computational complexity of the 3D model, animal burrows were modeled as a highly permeable soil ($k = 10^{-3}$ m/s) with negligible stiffness as compared with the surrounding soil. This condition was achieved by changing the properties of the levee material contained within the burrow geometries such that the new material would have insignificant resistance to deformation and water flow. This modeling approach eliminated numerical singularities that might have arisen if voids were to be explicitly modeled. It also enabled identical meshing for intact and deteriorated models. Quadratic tetrahedral 10-node elements allowed for the curvilinear modeling of the cylindrical cavities using a refined mesh around the burrows. The average element size of the mesh was 0.45 m, with elements on the order of 0.15 m in the refined area in the vicinity of the burrows. The total number of elements and nodes was 30 452, and 45 903, respectively. Table 1 summarizes the properties and parameters used in the analyses.

Seepage analysis

Figure 12 depicts the contours of pore pressure at cross sections taken at the centerline of the intact and deteriorated models. The calculated pore pressure at four different locations within the body of the levee are given in Table 2. The phreatic line of the LB model is somewhat similar to the intact model, with the dead end of the burrows dragging it further downward (Fig. 12b). The traced phreatic line for the LB model in the experiment (Fig. 7b) is in good agreement with that obtained using numerical analysis. Whereas pore pressures of LB are slightly lower than the intact model, the hydraulic gradients of the former are still higher. The pore pressure contours for the WB and LB models are quite dissimilar. For the WB model, higher pore pressure is noted in the burrow region as well as the foundation level. The near-horizontal extension of the contours is likely to be triggered by the burrow presence, similar to the traced phreatic line in Fig. 7c.

Figure 13 depicts the pore pressure distributions across the levee for three different elevations in the intact and deteriorated models. The results show that the increase in pore pressures is consistently and considerably higher for the WB compared with the LB and intact models. The increase was more pronounced near the landside slope. Compared with the intact model, the slightly lower phreatic line for the LB model resulted in a small decrease in pore pressures (Table 2). This general hydraulic performance for the deteriorated models is in fair agreement with the experimental observations expressed in terms of the arbitrarily defined hydraulic and normalized hydraulic gradients depicted in Figs. 6 and 8, respectively.

Stress analysis

The loss of structural strength within the body of the levee due to the presence of cavities is evident in the deteriorated models. To gain insight into the failure pattern and mechanism, the shear strain contours for the WB model are shown in Fig. 14a. The shear-strain bands for the WB model seem to occur along the failure surface. Additionally, strain concentrations extend along the burrow. The visually traced failure from the experiments (Fig. 14b) as well as the model geometry at failure (Fig. 14c) are qualitatively consistent with the numerical results. The progression of failure from the toe level toward the crest, as observed in the experiments, is intercepted by a weak plane at the burrow elevation. This observation can be linked to the horizontal cracks that appear at the landside slope (Fig. 10c) followed by excessive sliding (Fig. 10d). The loss of strength is further exacerbated by the increase in pore pressures in the toe area, where the failure surface begins (Fig. 12c). Further movement of the toe toward the landside deepens the horizontal cracks and eventually causes the observed toppling-like failure pattern (Figs. 10e and 10f).

Stability analysis

To investigate the effect of strength reduction on the stability of levee slopes, the strength-reduction method, where the soil strength is artificially weakened until the soil fails (Plaxis 2015), is used. This strength loss is modeled numerically by decreasing the cohesion and tangent of the friction angle in the same proportion

$$(3) \quad c'/c'_r = \tan\phi'/\tan\phi'_r = \text{strength-reduction ratio}$$

Fig. 12. Steady-state pore pressure distribution: (a) intact, (b) LB, and (c) WB. [Color online.]

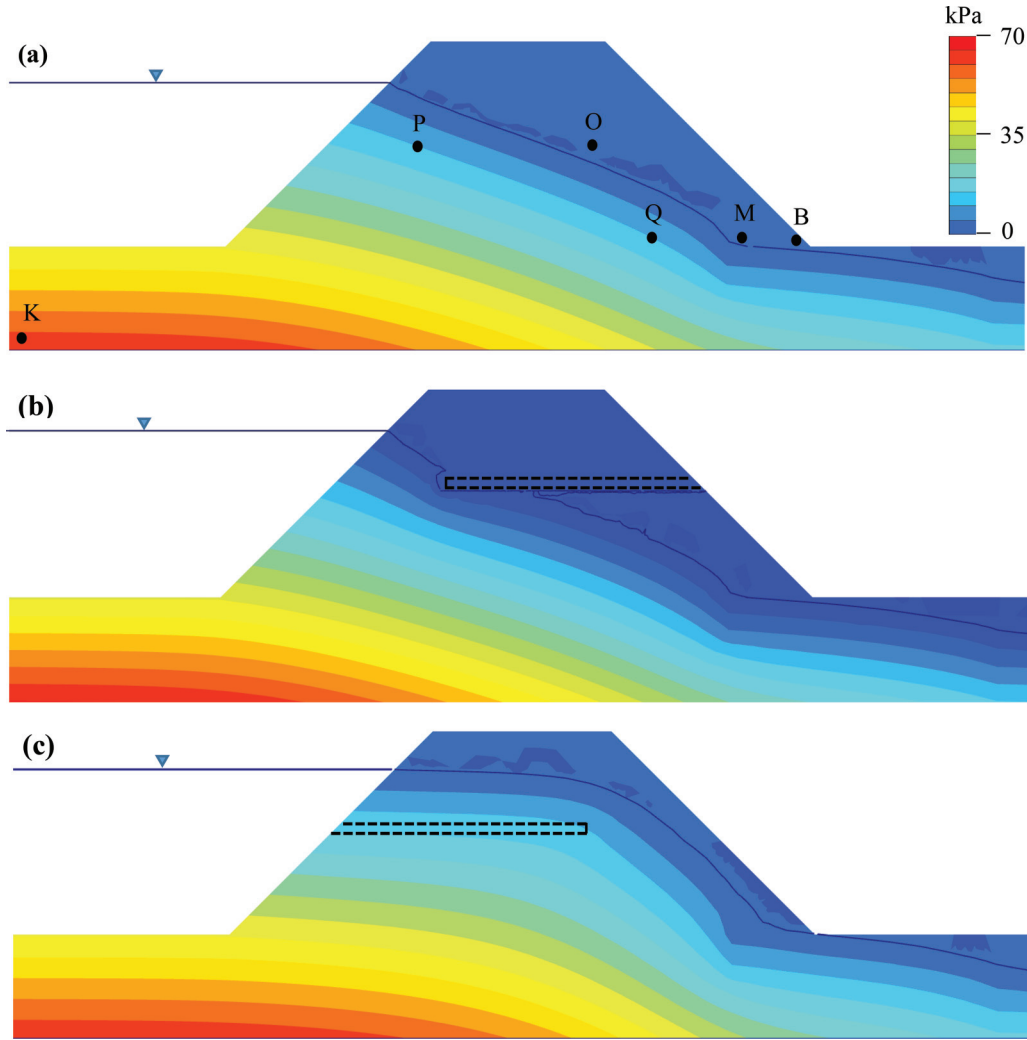


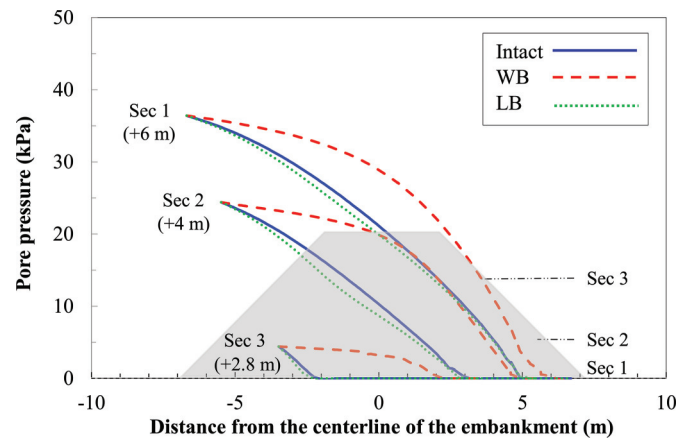
Table 2. Pore pressure comparison at selected points defined in Fig. 12.

Point	Pore-water pressure (kPa)		
	Intact	LB	WB
K	63.75	63.12	63.75
M	0	0	1.68
O	0	0	11.92
P	5.54	1.24	12.49
Q	7.57	8.4	13.94

where c' and ϕ' are the input strength parameters for the Mohr-Coulomb failure criterion and c'_r and ϕ'_r are reduced strength parameters that are just large enough to maintain equilibrium. In the FE model, no assumptions need to be made about the shape or location of the failure surface. Failure occurs through the zones within the soil mass in which the shear strength is unable to resist the applied shear stresses. Based on this approach and considering the toe of the landside slope as a reference point, the stability of both the intact and the deteriorated levees was investigated. Figure 15 demonstrates that the safety factors for the intact and LB levees were about 1.3, whereas the deteriorated WB levee was on the verge of failure with a factor of safety approaching 1.0.

The effect of the levee side slopes is numerically examined in Fig. 16. The slope angles were adjusted in three stages from 1H:1V

Fig. 13. Pore water pressure distribution at horizontal sections across levee. [Color online.]



to 3H:1V, and the safety factor versus slope instability was calculated for both the intact and the deteriorated levees. For the three geometries, mid-height burrows were introduced at the water-side, and the length of each burrow was gradually increased up to 75% of the levee width at that burrow's location. Results show that the introduction of burrows resulted in a general reduction in the

Fig. 14. Stress analysis of WB model: (a) shear strain ($\times 10^{-3}$), (b) side view of observed failure, and (c) top view of failed section. [Color online.]

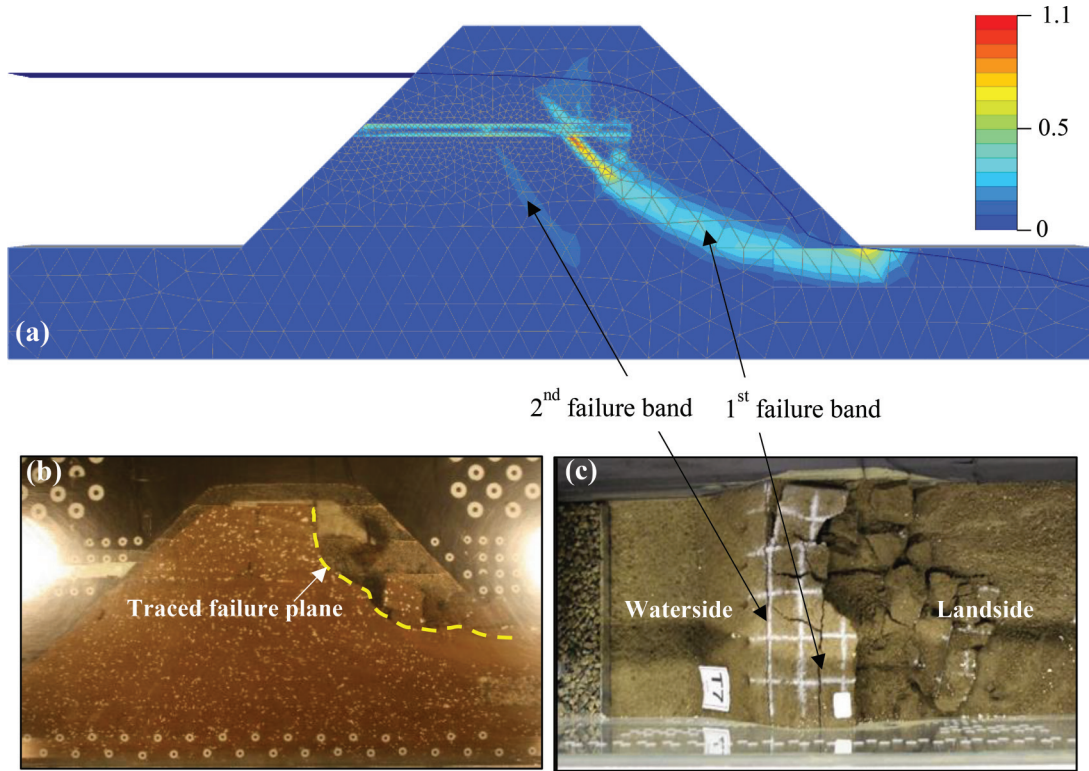
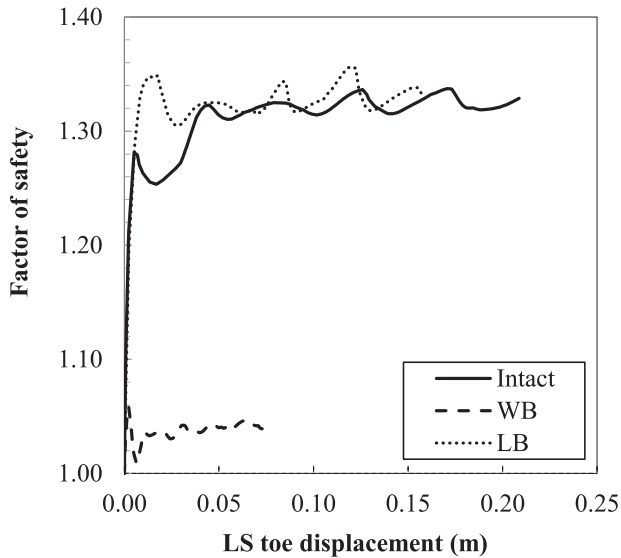


Fig. 15. Factor of safety of landside (LS) slope for LB and WB levees at time stamp $T = 6300$ s.

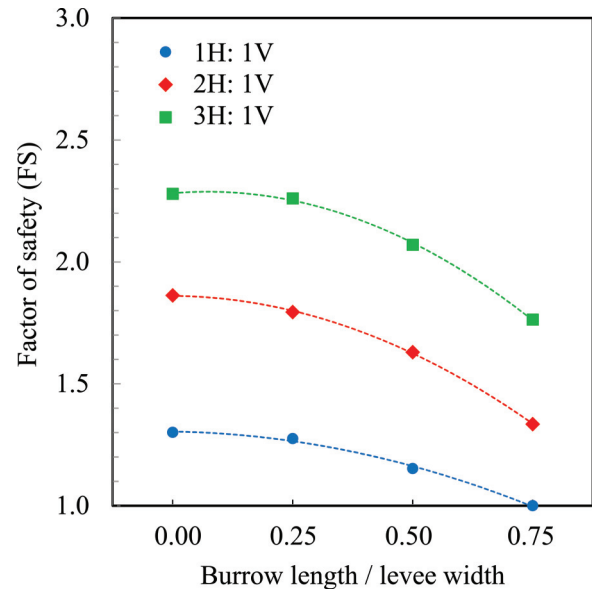


factor of safety. As the burrow length increased from 0% to 75% of the levee width, the factor of safety for the three investigated slopes — namely, 1H:1V, 2H:1V, and 3H:1V — decreased from 1.3, 1.85, and 2.3 to 1.0, 1.33, and 1.76, respectively. These results suggest that the adverse effect of the induced cavities is not limited to a specific geometry, and the reduction in the safety factor depends on the extent of the cavity into the levee.

Plausible failure mechanisms

Based on the experimental observations and numerical results, the following scenarios represent the authors' inferences about the progression of failure in the deteriorated levee models.

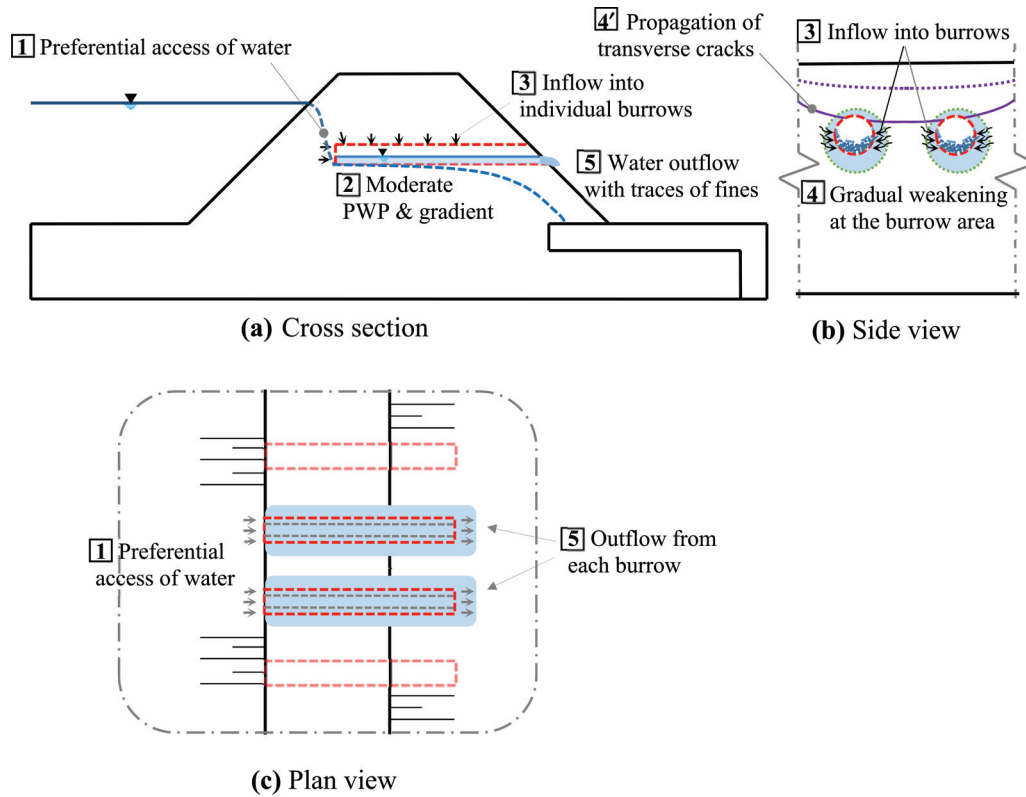
Fig. 16. Effect of side slopes on safety factor for levees with mid-height burrows. [Color online.]



Levee with landside burrows

Figure 17 proposes a progression of failure for the LB model with the perceived chronological order indicated by the boxes. The burrows evidently provide a preferential path for water flow toward the landside. Driven by the presence of cavities, the seeping water approaches the burrows from the closed end and the top, possibly carrying some fines. The analysis has shown that seepage into the burrows creates a concentrated flow around the burrows (see Fig. 17b). This flow makes the walls of the partially filled burrows vulnerable to erosion. The seeping water with the

Fig. 17. Proposed failure scenario for LB levee (sequence of distress events is indicated): (a) cross section; (b) side view; (c) plan view. [Color online.]



carried or washed fines exit on the landside end of the burrows, causing distress and disintegration of the surrounding area. This distress, coupled with the free water seepage at the burrow level, leads to structural deterioration locally propagating around individual burrows. Crest settlement starts to progress, with the development of the visible landside cracks between the burrows (Figs. 9b–9e). Eventually, the structural integrity of the burrows is completely jeopardized (Figs. 4 and 9f).

Levee with waterside burrows

A schematic of the proposed failure progression in the WB levee section is shown in Fig. 18. The burrows' proximity to water exacerbates flow and particle migration within the model and eventually weakens its structure. Unequivocally, this direct water access to the cavity system jeopardizes the hydraulic performance of the levee by raising the phreatic line. As compared with the LB case, the uninterrupted water entry obviously reduces head losses and yields considerably higher pore pressures (Fig. 13). The buildup of pore pressure — manifested in the higher phreatic line — is more intense because the water entering effortlessly at the waterside does not exit the burrow as easily. The “entrapment” of large pore pressures near the center of the model probably promotes transverse (lateral) seepage between the burrows. The lateral flow is associated with fines migration, causing disintegration and weakening in the zone between the burrows, which is manifested in the development of parallel cracks between the burrows. This flow pattern leads to erosion of the walls of the water-filled burrows. Subsidence develops across the levee section as adjacent burrows interact. As failure is approached, the high pore pressure leads to excessive seepage at the toe (Fig. 10b) and the initiation of the slip plane due to the loss of effective stress (shear strength). The intersection of the slip surface with the horizontal cracks around the burrow area forms a toe wedge (A in Fig. 18) and a middle wedge (B in Fig. 18). With further through-seepage, the toe wedge

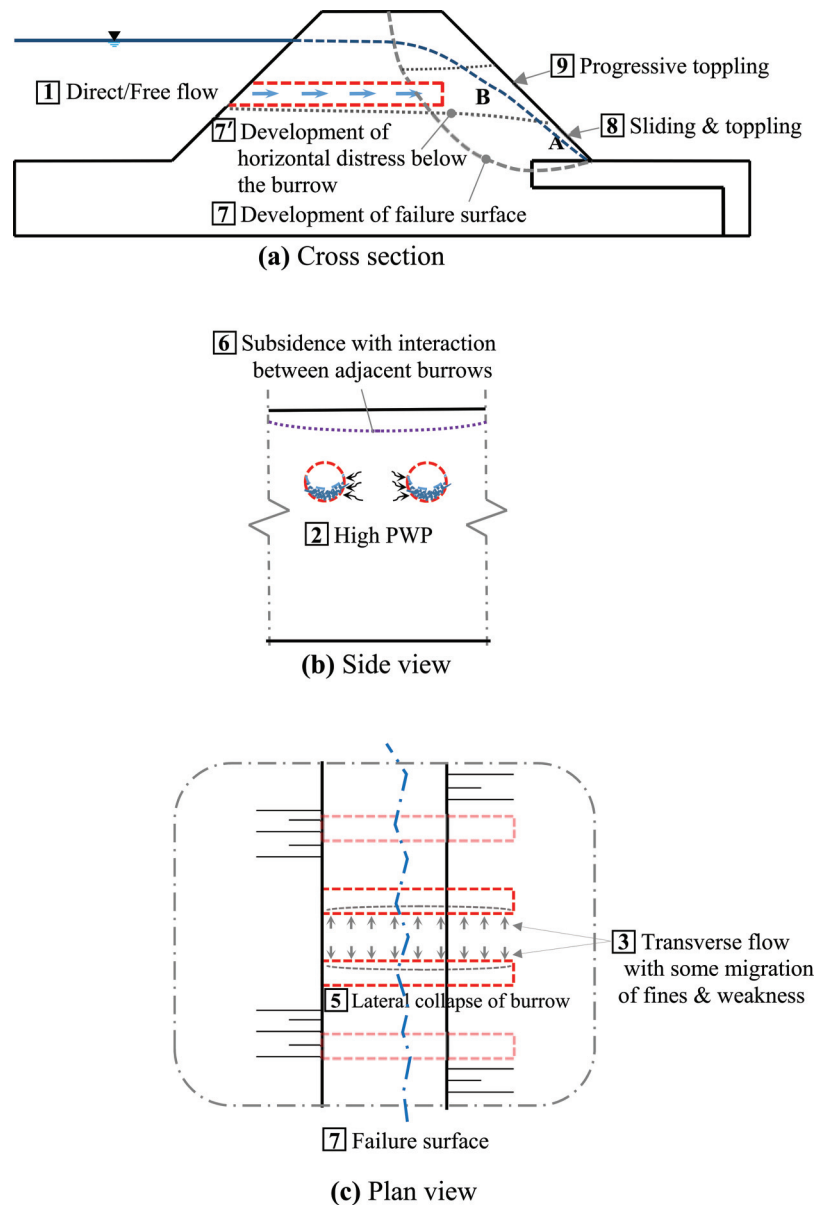
slides and topples, leading to crumbling of the middle wedge (Figs. 10c and 10d). Under the high “blocked” pore pressure, the complete and rapid washout of the levee section is inevitable. This mechanism justifies the near-instant crest subsidence at failure (Fig. 4).

Summary and closing thoughts

This study investigated the effect of idealized configurations of wildlife attack on the hydraulic performance and structural integrity of earth levees. Invasive animal damage was modeled as cylindrical cavities within levee models. A series of centrifuge experiments on scaled-down levee sections having waterside and landside burrows at different levels was conducted. For reference, an identical intact section underwent the same experiment. Compared with the intact levee, the deteriorated models exhibited a peculiar seepage pattern. The experimental results indicated that the presence of the introduced cavities has negative impacts on the hydraulic performance and stability of the levee. Using the centrifuge observations, this study postulated distinguishing failure mechanisms associated with attack side. Numerical simulations of the seepage and stress analysis further supported the proposed hydraulic response and failure mechanism. The effect of slope angles was numerically examined for three different side slopes — namely, 1H:1V, 2H:1V, and 3H:1V — with mid-height burrows. Results showed that the introduction of waterside burrows resulted in an average reduction in the factor of safety by about 25%.

The aforementioned findings collectively explain the unexpected and abrupt failures that could develop in levees deteriorated because of wildlife activities. The deduced failure scenarios suggest that subsidence in deteriorated levees is triggered by the combined effect of cavity destruction and loss of strength. Crest settlement (subsidence) can signify failure in deteriorated levees,

Fig. 18. Proposed failure scenario for WB levee (sequence of distress events is indicated): (a) cross section; (b) side view; (c) plan view. [Color online.]



which is indicative but does not provide a comprehensive view of the structural integrity. The levees' apparent intactness before failure could be misleading. This has significant bearing on levee system management, because the damage (size of cavities) of concealed burrow systems within a levee section could be much larger than what the visible openings suggest (Bayoumi and Meguid 2011).

The results reported in this study are limited by the investigated parameters, including the levee and burrow geometries. The size and density of the burrows could also be critical. Thus, generalization of the outcomes requires further investigation of other materials, geometrical features of earth structures, and deterioration levels and patterns.

Acknowledgements

This research is supported by the Natural Sciences and Engineering Research Council of Canada (NSERC) under grant number 311971-11. The assistance of the support staff at C-CORE centrifuge center in St. John's, Newfoundland, Canada, is highly appreciated.

References

Arulanandan, K., and Perry, E.B. 1983. Erosion in relation to filter design criteria for earth dams. *Journal of the Geotechnical Engineering Division, ASCE*, **109**(5): 682–698. doi:10.1061/(ASCE)0733-9410(1983)109:5(682).

ASTM. 2011. Standard practice for classification of soils for engineering purposes (Unified Soil Classification System). ASTM standard D2487. American Society for Testing and Materials, West Conshohocken, Pa. doi:10.1520/D2487-11.

Bayoumi, A., and Meguid, M. 2011. Wildlife and safety of earthen structures: a review. *Journal of Failure Analysis and Prevention*, **11**(4): 295–319. doi:10.1007/s11668-011-9439-y.

Blach, M., Jurist, K., and Morton, S. 2010. Anticipating California levee failure: Government response strategies for protecting natural resources from freshwater oil spills. U.S. Department of the Interior Office of Environmental Policy and Compliance, San Francisco, Region IX.

Bonelli, S., and Brivois, O. 2008. The scaling law in the hole erosion test with a constant pressure drop. *International Journal for Numerical and Analytical Methods in Geomechanics*, **32**(13): 1573–1595. doi:10.1002/nag.683.

Boukhemacha, M.A., Ioan, B., and Khoudir, M. 2011. Theoretical mathematical modeling for piping erosion near conduits. Vol. 7. Technical University of Civil Engineering, Bucharest, Romania.

Chlaib, H.K., Mahdi, H., Al-Shukri, H., Su, M.M., Catakli, A., and Abd, N. 2014. Using ground penetrating radar in levee assessment to detect small scale

- animal burrows. *Journal of Applied Geophysics*, **103**: 121–131. doi:10.1016/j.jappgeo.2014.01.011.
- Fell, R., Wan, C.F., Cyganiewicz, J., and Foster, M. 2003. Time for development of internal erosion and piping in embankment dams. *Journal of Geotechnical and Geoenvironmental Engineering*, **129**(4): 307–314. doi:10.1061/(ASCE)1090-0241(2003)129:4(307).
- FEMA. 2005. Technical manual for dam owners: impacts of animals on earthen dams. Federal Emergency Management Agency. Report No. FEMA 743.
- FEMA. 2011. Filters for embankment dams: best practices for design and construction. Federal Emergency Management Agency, U.S. Department of Homeland Security.
- Hori, T., Mohri, Y., and Niwano, K. 2007. Model tests for chemical injection to an outlet pipe of small earth dams. *In Proceedings of Japan Geotechnical Societies*, Japan.
- Plaxis, B.V. 2015. Plaxis 3D AE Version. 2015. Reference Manual. Delft, the Netherlands.
- Saghaee, G., Meguid, M.A., and Bayoumi, A. 2012a. An experimental procedure to study the impact of animal burrows on existing levee structures. *In Proceedings of the 2nd European Conference on Physical Modelling in Geotechnics*, Delft, the Netherlands, 23–24 April 2012.
- Saghaee, G., Meguid, M.A., and Bayoumi, A. 2012b. On the effects of animal burrows on the performance of homogeneous earthen structures. *In Proceedings of the GeoManitoba Conference*, Winnipeg, Manitoba, 30 September – 3 October 2012.
- Saghaee, G., Mousa, A., and Meguid, M. 2016. Experimental evaluation of the performance of earth levees deteriorated by wildlife activities. *Acta Geotechnica*, **11**(1): 83–93. doi:10.1007/s11440-015-0373-0.
- Schmocker, L., and Hager, W.H. 2012. Plane dike-breach due to overtopping: effects of sediment, dike height and discharge. *Journal of Hydraulic Research*, **50**(6): 576–586. doi:10.1080/00221686.2012.713034.
- Sellmeijer, H., de la Cruz, J.L., van Beek, V.M., and Knoeff, H. 2011. Fine-tuning of the backward erosion piping model through small-scale, medium-scale and IJkdijk experiments. *European Journal of Environmental and Civil Engineering*, **15**(8): 1139–1154. doi:10.1080/19648189.2011.9714845.
- Sharp, J.A., and McAnally, W.H. 2012. Numerical modeling of surge overtopping of a levee. *Applied Mathematical Modelling*, **36**(4): 1359–1370. doi:10.1016/j.apm.2011.08.039.
- Sherard, J.L., and Dunnigan, L.P. 1985. Filters and leakage control in embankment dams. *In Seepage and leakage from dams and impoundments*. Edited by R.L. Volpe and W.E. Kelly. American Society of Civil Engineers, New York. pp. 1–30.
- Sherard, J.L., Woodward, R.J., Gizienski, S.F., and Clevenges, W.A. 1963. Earth and earth-rock dams. John Wiley & Sons, New York.
- Taylor, R.N. 1995. Geotechnical centrifuge technology. Blackie Academic and Professional, London.
- van Beek, V.M., Knoeff, J.G., Rietdijk, J., Sellmeijer, J.B., and Cruz, J.L.D.L. 2010. Influence of sand and scale on the piping process - experiments and multivariate analysis. Paper presented at the Physical Modelling in Geotechnics Conference, Switzerland.
- van Beek, V.M., Knoeff, H., and Sellmeijer, H. 2011. Observations on the process of backward erosion piping in small-, medium- and full-scale experiments. *European Journal of Environmental and Civil Engineering*, **15**(8): 1115–1137. doi:10.1080/19648189.2011.9714844.
- White, D.J., Take, W.A., and Bolton, M.D. 2003. Soil deformation measurement using particle image velocimetry (PIV) and photogrammetry. *Géotechnique*, **53**(7): 619–631. doi:10.1680/geot.2003.53.7.619.
- Xu, F.G., Zhou, H.W., Zhou, J.W., and Yang, X.G. 2012. A mathematical model for forecasting the dam-break flood routing process of a landslide dam. *Mathematical Problems in Engineering*. **2012**: Art. 139642. doi:10.1155/2012/139642.
- Zhou, X., Jie, Y., and Li, G. 2012. Numerical simulation of the developing course of piping. *Computers and Geotechnics*, **44**: 104–108. doi:10.1016/j.compgeo.2012.03.010.